Journal of Power Sources 183 (2008) 717–723

Contents lists available at ScienceDirect

Journal of Power Sources

journal homepage: www.elsevier.com/locate/jpowsour

Electrospinning synthesis of C/Fe_3O_4 composite nanofibers and their application for high performance lithium-ion batteries

L. Wang, Y. Yu, P.C. Chen, D.W. Zhang, C.H. Chen *

Laboratory for Advanced Functional Materials and Devices, Department of Materials Science and Engineering, University of Science and Technology of China, Anhui Hefei 230026, China

ARTICLE INFO

Article history:
Received 31 March 2008
Received in revised form 5 May 2008
Accepted 26 May 2008
Available online 7 June 2008

Keywords:
Electrospinning
Composite
Nanofiber
Anode
Lithium battery

ABSTRACT

Carbon-based nanofibers can be used as anode materials for lithium-ion batteries. Both pure carbon nanofiber and C/Fe_3O_4 composite nanofibers were prepared by electrospinning and subsequent carbonization processes. The composition and structures were characterized by Fourier transformation infrared spectroscopy, X-ray diffraction, scanning and transmission electron microscopy. The electrochemical properties were evaluated in coin-type cells versus metallic lithium. It is found that after an annealing temperature of 500–700 °C, the carbon has disordered structure while Fe_3O_4 is nanocrystalline with a particle size from 8.5 to 52 nm. Compared with the pure carbon nanofiber, the 600 °C-carbonized C/Fe_3O_4 composite nanofiber exhibits much better electrochemical performance with a high reversible capacity of 1007 mAh g^{-1} at the 80th cycle and excellent rate capability. A beneficial powderization phenomenon is discovered during the electrochemical cycling. This study suggests that the optimized C/Fe_3O_4 composite nanofiber is a promising anode material for high performance lithium-ion batteries.

1. Introduction

In the last few decades, one-dimensional (1D) carbon materials such as carbon nanofiber, carbon nanotube, and composites based on these nanostructures have been widely investigated because of their applications in gas sensors [1,2], super-capacitors [3,4], field-emission microelectronic devices [5], catalysts [6,7] and lithium-ion batteries (LIBs) [8–10]. The methods to synthesize these 1D carbon-based materials include chemical vapor growth [11], template-assisted method [12] and electrospinning [13,14]. Among them, the electrospinning has been proved as an efficient and inexpensive way to fabricate carbon nanofibers and composite nanofibers. It is also noticed that the electrospinning method has been more and more often used to prepare polymer/inorganic composite systems in recent years [15]. For example, Lu et al. used electrospinning to prepare poly(vinyl pyrrolidone) nanofiber containing well dispersed semiconducting PbS nanoparticles [16]. With the inspiration of these studies, we consider it a feasible way to prepare carbon nanofibers with well-dispersed metal oxides particles by electrospinning of polymers and subsequent carbonization. This new category of composite materials should find wide applications in many fields, depending largely on which metal oxide component is in the nanofibers.

For lithium storage purpose, micrometer-sized carbon, either hard carbon or graphite, is a traditional anode material, which has been widely used in commercial LIBs owing to its stable capacity during cycling. Yet carbon nanofibers have not been well investigated for this application. On the other hand, nanosized transition metal oxides represent another type of promising alternative as the LIB anode material thanks to their very high capacity and interesting cycling performance [17–19]. Therefore, it is worthwhile to investigate a nanoscale carbon/metal oxide composite as the electrode material, which may combine the merits of both components.

In this work, C/Fe_3O_4 nanofibers are prepared and evaluated as anode material for high performance LIBs. The ferriferrous oxide (Fe_3O_4) is selected for its high theoretical capacity (924 mAh g^{-1}), low cost and environmental friendliness. Also, the composite fiber is designed for two purposes: on one hand, the carbon component and fibrous morphology of nanofibers can digest the volume change during the conversion reaction [20–22]; on the other hand, we have recently identified a C/Co composite nanofiber as an excellent electrode material [23]. The metallic cobalt is believed to serve as a conductive additive to improve the electronic conductivity of the nanofiber. Nevertheless, the addition of the electrochemically inactive cobalt leads to an energy density loss of the cell. Therefore, here we employ in the composite the electrochemically active Fe_3O_4 nanoparticles that can also act as a conductive addi-

* Corresponding author. Tel.: +86 551 3606971; fax: +86 5513601592.
E-mail address: cchchen@ustc.edu.cn (C.H. Chen).

0378-7753/$ – see front matter © 2008 Elsevier B.V. All rights reserved.
doi:10.1016/j.jpowsour.2008.05.079

tive when it is reduced to metallic iron during the lithium insertion. The experimental results indicate that the optimized C/Fe_3O_4 composite nanofiber can indeed deliver a very high reversible capacity together with excellent rate capability.

2. Experimental

A typical electrospinning method was adopted to fabricate carbon fiber or C/Fe_3O_4 fibers. About 0.75 g polyacrylonitrile (PAN) (M.W. 86,000) was dissolved in 10 mL *N*,*N*-dimethyformatide (DMF) to form a polymer precursor, which was used to prepare carbon nanofiber. At the same time, 1.3 g ferric acetylacetonate ($Fe(acac)_2$) was added into the polymer solution as a precursor for electrospinning of C/Fe_3O_4 fibers. During the electrospinning process, the precursor solution was transported to a metal needle with a flow rate of 4 μL min^{-1} by a syringe pump. A flat copper foil used as a fiber collector was put about 12 cm away under the needle. A positive direct current (DC) voltage of about 12–14 kV was applied between the needle and the collector to generate a stable continuous PAN-based nanofiber that was collected on the foil. Similarly, a PAN nanofiber was also prepared without adding $Fe(acac)_2$ in the precursor solution. Then the electrospun fibers were pre-oxidized in air at 240 °C for 6 h in a furnace. This pre-oxidation process was to protect the fibrous morphology of the nanofibers. After the pre-oxidation step, a carbonization treatment was conducted at 500, 550, 600 and 700 °C, respectively, under argon atmosphere for 10 h. After this step, either pure carbon nanofibers or C/Fe_3O_4 composite nanofibers were obtained. To obtain the carbon yield quantitatively, the PAN nanofiber and its 600 °C-derived carbon nanofiber were weighted just before the pre-oxidation and after the carbonization process.

The electrospun PAN nanofiber and its derived pure carbon and C/Fe_3O_4 nanofibers were analyzed by Fourier transform infrared spectroscopy (Bruker EQUINOX55). They were also characterized by X-ray diffraction (Philips X'pert Pro Super, Cu Kα radiation). The morphology of these nanofibers was examined with a scanning electron microscope (SEM) (Hitachi X-650) and a transmission electron microscope (TEM) (FEI Tecnai F20 operating at 20 kV) with a function to perform selected area electron diffraction (SAED).

The electrochemical properties of the nanofibers were characterized using 2032 coin cells with metallic lithium as the counter electrode. These carbon-based nanofibers were adhered onto a copper foil with a PVDF binder to make working electrodes. The weight ratio of the active materials and the binder was controlled as 10:1. The electrolyte was 1 M $LiPF_6$ in ethylene carbonate/dimethyl carbonate (1:1, v/v). The cells were assembled in an argon-filled glove box (MBRAUN LABMASTER 130) with moisture and oxygen levels less than 1 ppm. They were cycled in the voltage range between 3.0 and 0.01 V on a multi-channel battery cycler (NEWWAEE BTS-610). The AC impedance spectra of the cells after different cycles were measured on an electrochemical workstation (CHI 604B) with the frequency range from 0.01 Hz to 100 kHz. Some of the cells were disassembled after electrochemical cycling and the nanofiber electrodes were washed by diethylene carbonate and *N*-methyl-pyrrolidone before they were observed by SEM.

3. Results and discussion

3.1. Structural and compositional characterizations

Fig. 1 shows the micro-images of as-electrospun poly(acrylonitrile) (PAN) fiber before the pre-oxidation step and the final products carbon fiber and the 600 °C-treated C/Fe_3O_4 composite fiber. Except for a few of beads-like particles originated from the instability during electrospinning, most PAN fiber is rather homogeneous in thickness and lies randomly on the copper foil collector (Fig. 1a). It can be seen under a larger magnification that the fiber has a smooth surface and a diameter in the range of 350–400 nm (Fig. 1b). After the pre-oxidation at 240 °C in air and carbonization at 600 °C in argon, we obtained a carbon nanofiber shown in Fig. 1c. Compared with the PAN fiber from which it derives, the carbon nanofiber looks thinner, which may be due to the volume shrinkage of PAN because of the weigh loss during the carbonization. Our experiment indicates that there is about 50% weigh loss when the polymer fiber is carbonized at 600 °C for 10 h. If the precursor solution for the electrospinning contains ferric acetylacetonate, an iron-oxide/carbon composite fiber is also obtained with the same heat treatment procedure (Fig. 1d). The composition of this fiber is identified as C/Fe_3O_4 composite (see the XRD results below). Obviously, it is about 350 nm in diameter, which is similar to the previous two fibers. Also, it must be more fragile due to the presence of Fe_3O_4. Considering the carbon yield rate of about 50% for the PAN fiber and a complete decomposition of ferric acetylacetonate into iron-oxide, the C-Fe_3O_4 mass ratio can be calculated as 69:31.

The FT-IR spectra of the PAN nanofiber, 500 °C-carbonized carbon nanofiber and C/Fe_3O_4 composite nanofibers are shown in Fig. 2. Before the thermal treatment, the polymer fiber shows a typical IR spectrum of PAN (spectrum a), which is almost the same as Serkov's results [24]. After the 500 °C treatment, all of the absorption bands of PAN disappear, indicating that the PAN has totally transformed into carbon (spectrum b). On the other hand, for both of the carbon fiber and C/Fe_3O_4 fiber (spectra b and c), there are only two weak absorption bands at 1600 and 3440 cm^{-1}, which are attributed to the presence of water that is usually brought into samples from air during the IR measurement. It is noticed that, compared with the pure carbon fiber (spectrum b), only one more absorption band near 590 cm^{-1} is visible for the sample of C/Fe_3O_4 fiber (spectrum c), and it can be attributed to the presence of Fe_3O_4 [25]. Due probably to the co-existence of carbon in the sample and the carbon content is more than that of Fe_3O_4 both in mass and volume, this absorption signal near 590 cm^{-1} is not very strong. Based on the above results, we can deduce that the ferric acetylacetonate contained in the PAN fiber has been totally decomposed into iron-oxide.

Fig. 3 shows the XRD patterns of the pure carbon fiber and the C/Fe_3O_4 composite fibers obtained at four different temperatures from 500 to 700 °C. For the pure carbon nanofiber, only two broad and weak diffraction peaks of (0 0 2) and (0 0 4) peaks are detected (Fig. 3a). According to Sandi et al. [26], the carbon obtained in our experiment should be disordered carbon. On the other hand, for the iron-containing composite fibers, the fibers obtained at different temperatures show distinctly different XRD patterns from the carbon fiber (Fig. 3b). Unlike the pure carbon fiber, six diffraction peaks at 18.1°, 30.2°, 35.5°, 43.1°, 56.9° and 62.7° are detected, which correspond to the diffraction peaks of (1 1 0), (2 2 0), (3 1 1), (2 0 8), (5 1 1) and (4 4 0) of Fe_3O_4 (JCPDS 85-1435). Furthermore, with increasing the temperatures of the carbonization, these diffraction peaks become stronger and the breadth of the peaks becomes narrower. These changes indicate that the Fe_3O_4 particles obtained at a higher temperature are better crystallized with larger crystallite sizes. Thus, the Fe_3O_4 particles contained in the composite fiber obtained at 700 °C has the largest particle size. According to a calculation by Scherrer equation (Table 1), the crystallite size of Fe_3O_4 in the composite fibers obtained at 500 and 700 °C is 8.5 and 52.0 nm, respectively (Table 1).

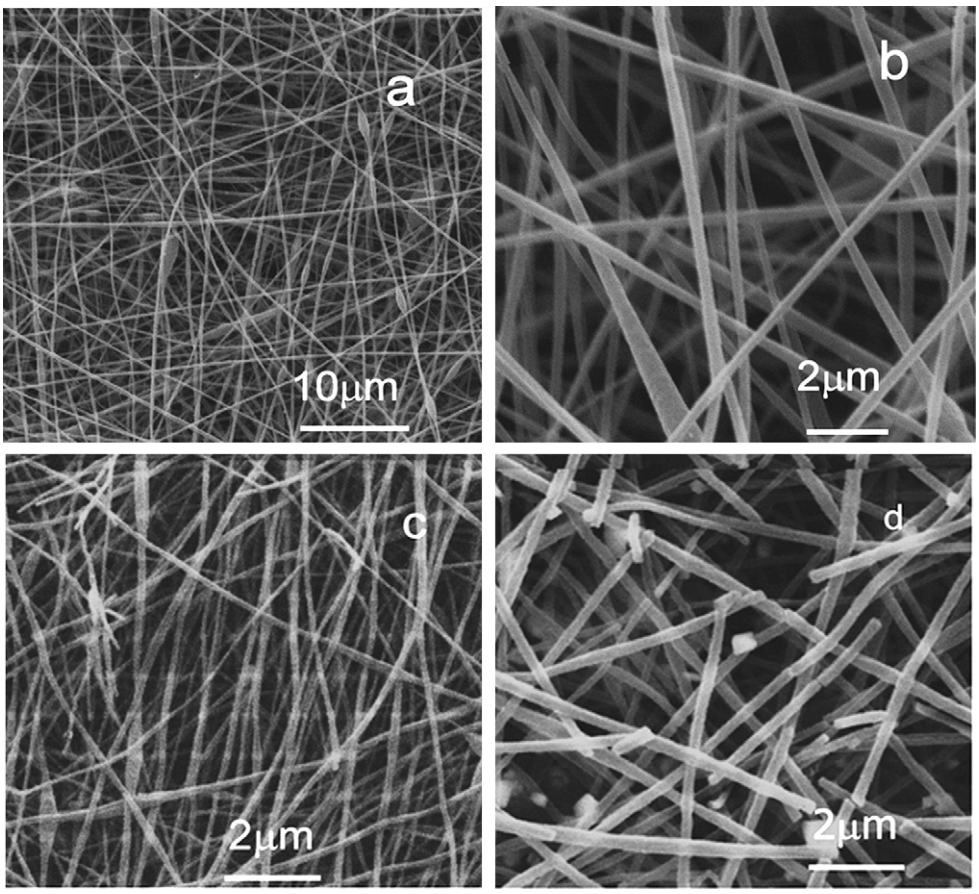

Fig. 1. SEM images of a PAN nanofiber before the pre-oxidation step (a and b), a 600 °C-carbonized carbon nanofiber (c) and a C/Fe_3O_4 composite nanofiber (d).

In order to further identify the nano-phase nature of the Fe_3O_4 particles contained in the composite fibers, the HRTEM image and SAED patterns of 600 °C-treated composite fiber are shown in Fig. 4. It can be clearly seen that nanosize particles with an average diameter of 20 nm are dispersed in the fiber (Fig. 4a), and the SAED pattern (inset image in Fig. 4a) is comprised of a well-resolved set of concentric rings with bright spots, indicating the nanocrystalline nature of the Fe_3O_4. The d-spacing of the planes in the HRTEM lattice image (Fig. 4b) is 2.94 Å, which is in good agreement with the d-spacing of (2 2 0) plane for Fe_3O_4. We can also see that the carbon around the Fe_3O_4 particle is indeed with a disordered lattice structure.

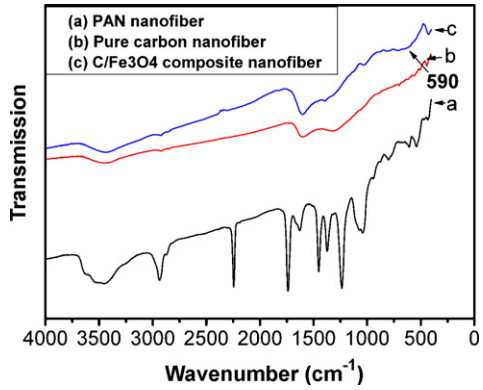

Fig. 2. Fourier transformation IR spectra of the electrospun PAN nanofiber, 500 °C-carbonized carbon nanofiber and C/Fe_3O_4 composite nanofiber.

Table 1
The particle size of Fe_3O_4 nanocrystals in the C/Fe_3O_4 composite nanofibers carbonized at different temperatures calculated by the Scherrer equation, $D = 0.89\lambda/(\beta \cos\theta)$, where 2θ stands for the diffraction angle of (3 1 1) peak, β the peak width at half height and D the crystallite size

Temperature (°C)	2θ (rad)	β (rad)	D (nm)
500	0.6199	0.0171	8.5
550	0.6266	0.0171	8.5
600	0.6215	0.0085	17.1
700	0.6205	0.0028	52.0

3.2. Electrochemical properties of carbon and C/Fe_3O_4 nanofibers

Because both carbon and Fe_3O_4 can be used as the electrode materials for reversible lithium storage either in batteries or in super capacitors, it is interesting to investigate the electrochemical performance of the carbon nanofiber and the C/Fe_3O_4 composite nanofiber prepared in this study. Fig. 5 shows the charge–discharge behavior of lithium half cells C/Li and C(Fe_3O_4)/Li with the nanofibers as working electrodes versus lithium. It can be seen from the voltage profiles of the first cycle (Fig. 5a) that the carbon nanofiber carbonized at 600 °C shows a typical discharge–charge characteristics of disordered carbon [27]. However, for the C/Fe_3O_4 composite nanofibers, the cells show different voltage profiles with a long plateau at about 0.75 V in the discharge (lithiation) process and a short plateau at about 1.5 V in the charge (delithiation) process. The voltage plateaus measured here must be due to the presence of Fe_3O_4 and the heterogeneous reaction between lithium and metal oxide $8Li + Fe_3O_4 \leftrightarrows 3Fe + 4Li_2O$ [28,29]. In fact, the discharge profiles above 0.7 V can be divided

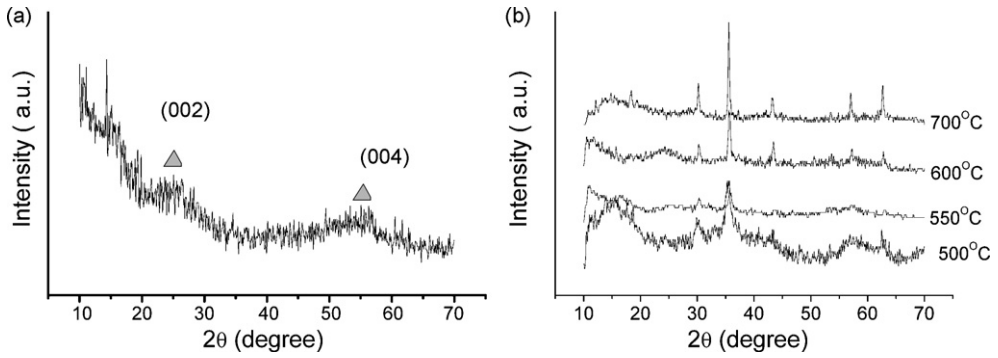

Fig. 3. XRD patterns of 600 °C-carbonized carbon nanofiber (a) and C/Fe_3O_4 composite nanofibers annealed at different temperatures from 500 to 700 °C (b).

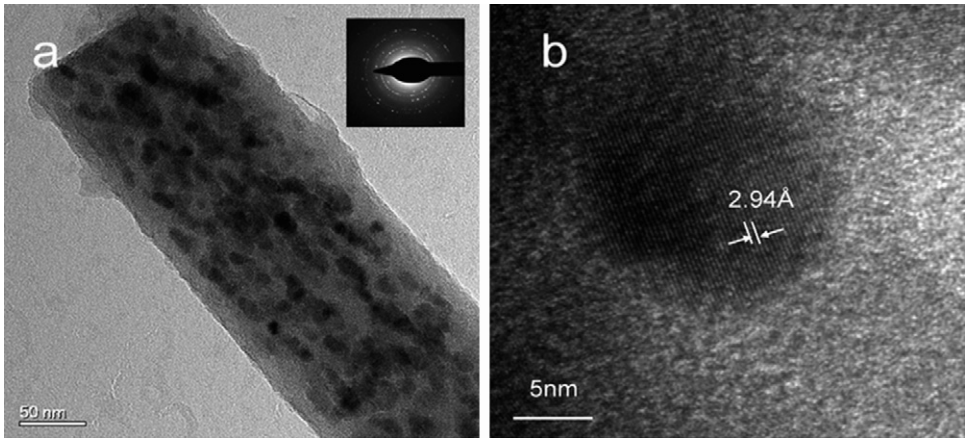

Fig. 4. TEM photographs of a 600 °C-carbonized C/Fe_3O_4 nanofiber: (a) TEM image at low resolution and SAED pattern (inset image); (b) high resolution lattice image.

into two segments, i.e. a sloping part from about 2.0 to 0.75 V, and a plateau at 0.75 V. The former can be attributed to the reaction $Fe_3O_4 + xLi \rightarrow Li_xFe_3O_4$; the latter corresponds to the conversion reaction $Li_xFe_3O_4 + (8 - x)Li \rightarrow 3Fe + 4Li_2O$. The plateaus are not pronounced for the C/Fe_3O_4 nanofibers carbonized at the lower temperatures 500 and 550 °C because the particle size of Fe_3O_4 in these electrodes is very small (8.5 nm) compared with those in the 600 °C- and 700 °C-carbonized composite samples (17.1 and 52.0 nm) (Table 1). Also, the capacity associated with the high voltage sloping part (or x value in the above reaction) decreases with increasing the carbonization temperature.

Fig. 5b shows the cycling performance of the carbon-based nanofibers in this study. For the pure 600 °C-carbonized carbon nanofiber delivers a first-cycle discharge capacity of 1041 mAh g^{-1}. The 600 °C-carbonized C/Fe_3O_4 nanofiber exhibits the largest discharge capacity of 1551 mAh g^{-1} in the first cycle, while the composite fibers carbonized at 500, 550, 700 °C deliver a capacity of 1318, 1151 and 957 mAh g^{-1}, respectively. It is well established that a disordered carbon obtained at a relatively low temperature (<1000 °C) has a large capacity but with low electronic conductivity [30,31]. The lower the annealing temperature is, the more defects on the surface of the carbon that allow more lithium to store. On the other hand, a disordered carbon has a low electronic conduc-

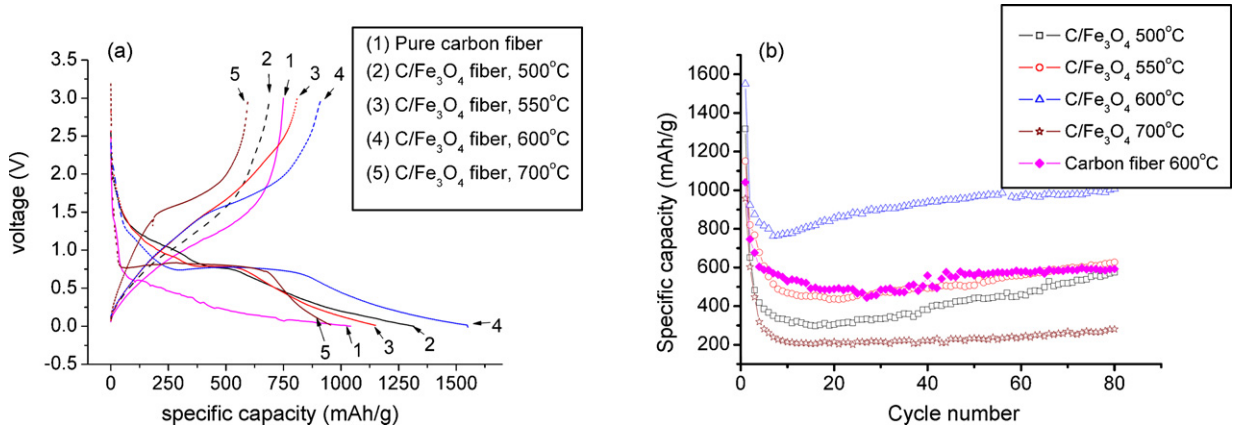

Fig. 5. Electrochemical tests of C/Li or C(Fe_3O_4)/Li half cells: (a) voltage profiles of the 1st cycle; (b) discharge capacity versus cycles of the nanofibers. The pure carbon fiber (curve 1) was obtained at 600 °C. The current density was all around 200 mA g^{-1}.

tivity compared with that of a graphitic carbon. For a carbon-based composite material, three factors can be considered to determine its capability of lithium storage: electronic conductivity, concentration of surface defects and the interfacial area between the two components. Thus, this is why the 600 °C-carbonized C/Fe_3O_4 nanofiber gives rise to the highest capacity because it reaches a good compromise among these three factors. When the annealing temperature is raised to 700 °C, the capacity of its carbon component decreases considerably (only 300 mAh g^{-1} according to Kim's results [32]). Also, the Fe_3O_4 particle grows from 17 to 52 nm (Table 1). For the 500 °C- and 550 °C-carbonized composite fibers, the comparatively poor electronic conductivity limits the capacity. Note that the reversible capacity of the 600 °C-carbonized C/Fe_3O_4 nanofiber reaches about 1000 mAh g^{-1} at the 80th cycle, which is significantly higher than that of the state-of-the-art anode material graphite (around 340 mAh g^{-1}).

Another difference between the pure carbon nanofiber and the C/Fe_3O_4 nanofibers is noticed on their capacity changes with cycling in Fig. 5b. The capacity of the pure carbon nanofiber keeps virtually stable after some degree of lowering in the first 40 cycles or so. The first stage of capacity decrease may be explained by the structure re-organization of the carbon [33]. On contrast, all of the C/Fe_3O_4 composite nanofibers experience a gradual capacity rise from 10th cycle to the end of the measurement (80th cycle). Specifically, for the 600 °C-carbonized composite nanofiber, it reaches a minimum of 763 mAh g^{-1} at the 7th cycle and rises to 1007 mAh g^{-1} at the 80th cycle. Similarly, the capacity decrease in the first 10 cycles can be also related to the above structure re-organization of the carbon component.

3.3. Morphology changes of nanofibers after electrochemical cycling

To explore the course of the capacity rise of those composite nanofibers, we examined their morphology change after electrochemical cycling. The SEM photos of the nanofibers after 80 cycles are shown in Fig. 6. It can be seen that the pure carbon nanofiber retains its original morphology (Fig. 6a), i.e. most of the fiber is with smooth surface and about 300 nm in diameter. On the other hand, a marked morphology change is found for the composite nanofibers (Fig. 6b and c). In general, the fiber becomes powderized. For the part that is on the surface of the electrode, many little particles are loosely agglomerated and arranged in the lines where supposed to be the fiber (Fig. 6b). For the part that is in contact with the copper foil current collector, however, the powderization phenomenon is more substantial (Fig. 6c) so that the fibrous morphology has almost disappeared. Apparently, during the lithium insertion and extraction in the composite nanofibers, a large volume change must have taken place. Such a volume expansion and shrinkage can lead to the breaking of the fibers into small particles. It can be calculated that when Fe_3O_4 is reduced completely into Fe by lithium, the volume should increase theoretically by 80.8%. Another factor that induces the powderization of the fiber is related to the presence of highly conducting iron produced in situ after deeply discharging the cell down to a low voltage below 0.8 V. The iron inclusion should enhance the electronic conduction along the C/Fe interface and thus further activate the carbon component for lithium insertion. This is also likely one of the reasons why the 600 °C-carbonized composite nanofiber has a higher capacity than the 600 °C-carbonized pure carbon nanofiber as shown in Fig. 5.

With regard to the difference in the degree of powderization on the two sides of the fiber electrode, it can be explained by the difference in the strain release. Because of the restriction of the current collector, the strain caused by the volume change cannot be released easily on the fiber electrode side that is in contact with the current collector and the powderization is so much that the original fibrous structure is smeared out. To the contrary, the easy release of the strain on the other side of the fiber electrode makes the fibrous structure be retained during the powderization on cell cycling. Another possible reason for the difference in powderization between the current collector side and the other side might be related to the transient potential difference in these two locations during cell cycling. The potentials are lower in discharging and higher in charging in the vicinity of current collector side compared to the other side. Such a potential difference may cause different powderization behavior of the electrode. Nevertheless, the exact cause of such a phenomenon needs to be investigated further in the future work.

Note that the powderization effect here does not cause negative impact on the electrochemical performance of the nanofiber electrodes. It actually improves the cycling property by increasing the effective surface area of the electrodes and accommodating the inevitable periodical volume change during lithium insertion and extraction. Such an improvement effect caused by the powderization has been also confirmed in the Cu_2O–Li_2O composite system [34,35].

3.4. Impedance and rate capability of nanofiber electrodes

In order to find out whether the electrical conduction can be improved by the addition of Fe_3O_4 in the carbon nanofibers and how the impedance changes with cycling, AC impedance test was conducted on two half cells with the 600 °C-carbonized carbon nanofiber and 600 °C-carbonized C/Fe_3O_4 composite nanofiber as the working electrodes. The cells were first charged–discharged for 5 and 100 cycles and then fully discharged to 0.01 V prior to the measurement. The difference is clearly seen in their impedance spectra (Fig. 7). Both of the cells exhibit a typical impedance spectrum of a rechargeable lithium cell; it is consisted of two semicircles in the high and medium frequency ranges and a straight line in the low-frequency range. The two semicircles can be ascribed to the charge-transfer processes on the interfaces between the electrolyte and the nanofiber electrode or the metallic lithium counter electrode. The straight line is due to the lithium-ion diffusion and accumulation process in the working electrodes. Different from the Warburg impedance which usually exhibits a 45°-slope straight line, the straight line branch observed here seems due to capacitance components, and similar result is observed in Gnanaraj's study on using hard carbon as the electrode material [33]. Therefore, this capacitive behavior should be related to lithium storage in the micropores of disordered carbon. It is also noticed that both the carbon nanofiber and the C/Fe_3O_4 composite nanofiber exhibit the same trend upon increasing the cycle number, i.e. the cell impedance decreases substantially with cycling. After 100 cycles, the total charge transfer resistance of these two cells decreases from 640 to 200 Ω and from 400 to 130 Ω, respectively. On one hand, the reduced resistance of deep-discharged C/Fe_3O_4 composite nanofiber compared to the pure carbon nanofiber should be related to the generation of iron during the electrochemical reaction. On the other hand, combined with the cycling performance (Fig. 5b), this resistance decrease may also be related to the wetting process between the nanofibers and the liquid electrolyte. Basically, the wettability of nonpolar carbon materials by the polar liquid electrolyte is not very good, especially if there are some dangling hydrogen–carbon bonds on the surface of the carbon nanofibers due to incomplete carbonization of PAN fibers [36]. The addition of inorganic polar Fe_3O_4 in the composite should enhance the wettability of the electrode. Thus, the impedance of the C(Fe_3O_4)/Li cell is considerably lower than that of the C/Li cell at the 5th cycle (Fig. 7). After 100 cycles, the dangling hydrogen atoms may have been

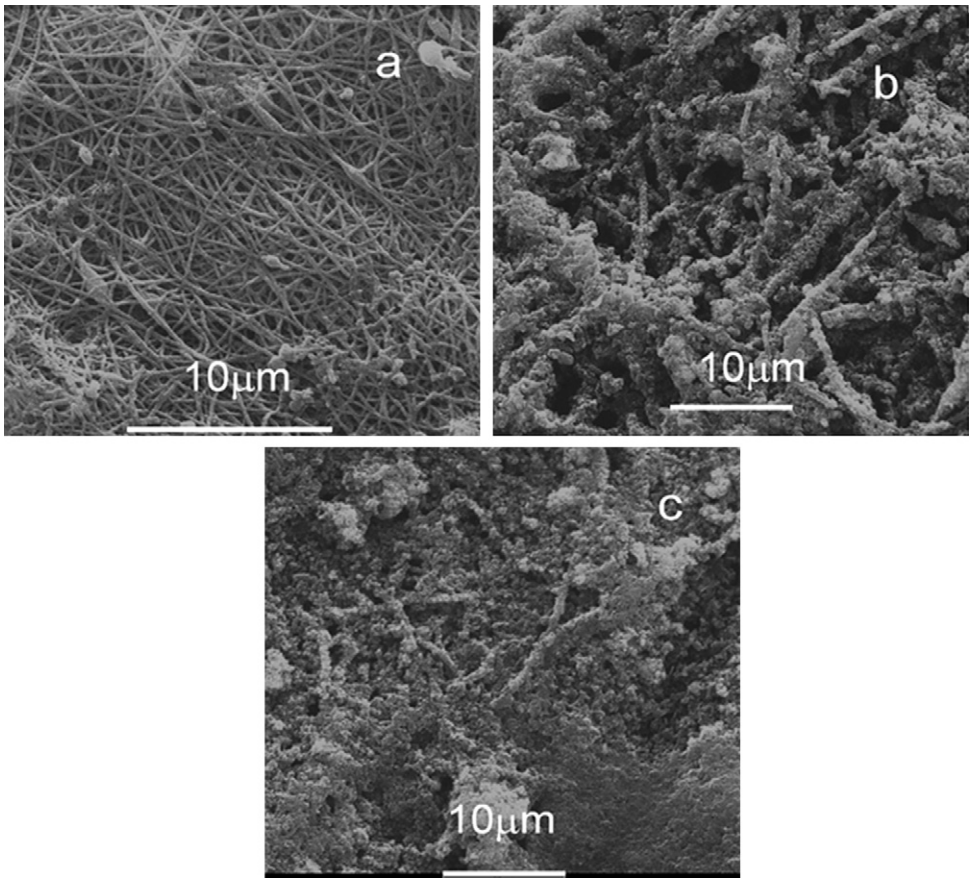

Fig. 6. SEM photos of a 600 °C-carbonized pure carbon nanofiber (a) and a C/Fe_3O_4 nanofiber after 80 cycles (b and c). For C/Fe_3O_4, the morphology of the side on the surface (b) is different from that of the side in contact with the copper foil current collector (c).

removed from the surface by the electrochemical reaction, which leads to the enhancement of wettability and hence the decrease of the cell impedance. Of course, the powderization effect should be another reason for the lower impedance in the composite electrode than in the pure carbon electrode at the 100th cycle.

Besides high capacity, rate capability is also important for the electrode materials for high performance LIBs. Fig. 8 shows the voltage profiles of the 600 °C-carbonized C/Fe_3O_4 nanofiber cycled at different current density. Before this measurement, the cell had been cycled for 100 times at 200 mA g^{-1}, and then it was cycled under different current density range from 200 to 1600 mA g^{-1}. It can be seen that the composite nanofiber delivers a capacity of 1096 mAh g^{-1} at a low current density of 200 mA g^{-1}. When the current density increases to 400 mA g^{-1}, the voltage profile seems to be overlapped with the one obtained at 200 mA g^{-1}, and there is only a little capacity loss of 74 mAh g^{-1}. Even under a high current density of 1600 mA g^{-1}, the composite nanofiber can also deliver a high capacity of 623 mAh g^{-1}, which is much higher than the common carbon materials. This result suggests that this C/Fe_3O_4 composite nanofiber represents a promising candidate of anode material for high performance LIBs which can be used in (hybrid) electric vehicles and electric tools.

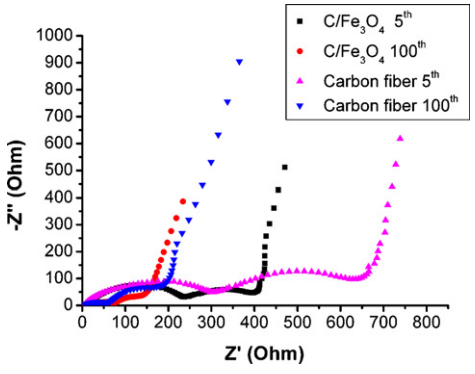

Fig. 7. AC impedance spectra of the C/Li and C(Fe_3O_4)/Li half cells after 5 and 100 cycles. All the cells were discharged to 0.01 V and measured in a frequency range from 0.01 Hz to 100 kHz.

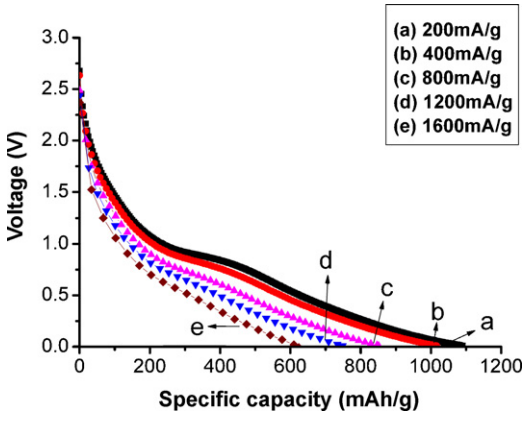

Fig. 8. Discharge voltage curves of a 600 °C-carbonized C/Fe_3O_4 nanofiber at different current densities after 100 cycles.

4. Conclusions

A novel C/Fe_3O_4 composite nanofiber has been prepared by electrospinning of PAN-based nanofibers and subsequent carbonization. At an annealing temperature below 700 °C, the carbon obtained is with disordered structure while the Fe_3O_4 is nanocrystalline with an average particle size between 8.5 and 52.0 nm. An in-depth electrochemical study reveals that the C/Fe_3O_4 composite nanofiber obtained at 600 °C exhibits a high reversible capacity, good cycling performance and excellent rate capability. The addition of Fe_3O_4 in the composite plays an important role in increasing the effective surface area, enhancing the electronic conductivity and improving the wettability of the electrode. These superior electrochemical properties of the composite nanofiber indicate that this unique composite may find promising applications in high performance Li-ion batteries.

Acknowledgements

This study was supported by National Science Foundation of China (grant no. 50372064 and 20471057). We are also grateful to Dr. Ingo Lieberwirth from Max-Plank Institute at Mainz for TEM measurement.

References

[1] J. Jang, J. Bae, Sens. Actuators B 122 (2007) 7–13.
[2] J. Li, Y.J. Lu, Q. Ye, M. Cinke, J. Han, M. Meyyappan, Nano Lett. 3 (2003) 929–933.
[3] K. Honda, M. Yoshimura, K. Kawakita, A. Fujishima, Y. Sakamoto, K. Yasui, N. Nishio, H. Masuda, J. Electrochem. Soc. 151 (2004) A532–A541.
[4] D.N. Futaba, K. Hata, T. Yamada, T. Hiraoka, Y. Hayamizu, Y. Kakudate, O. Tanaike, H. Hatori, M. Yumura, S. Iijima, Nat. Mater. 5 (2006) 987–994.
[5] K.B.K. Teo, M. Chhowalla, G.A.J. Amareatunga, W.I. Milne, G. Pirio, P. Legagneux, F. Wyczisk, D. Pribat, D.G. Hasko, Appl. Phys. Lett. 80 (2002) 2011–2013.
[6] C. Park, R. Terry, K. Baker, J. Phys. Chem. B 102 (1998) 5168–5177.
[7] E.S. Steigerwalt, G.A. Deluga, D.E. Cliffel, C.M. Lukehart, J. Phys. Chem. B 105 (2001) 8097–8101.
[8] M.S. Wu, J.T. Lee, P.C.J. Chiang, J.C. Lin, J. Mater. Sci. 42 (2007) 259–265.
[9] S.H. Yoon, C.W. Park, H. Yang, Y. Korai, I. Mochida, E.T.K. Baker, N.M. Rodriguez, Carbon 42 (2004) 21–32.
[10] X.X. Wang, J.N. Wang, H. Chang, Y.F. Zhang, Adv. Funct. Mater. 17 (2007) 3613–3618.
[11] W.E. Alvarez, B. Kitiyanan, A. Borgna, D.E. Resasco, Carbon 39 (2001) 547–558.
[12] T. Maiyalagan, B. Viswanathan, Carbon 93 (2005) 291–295.
[13] H.Q. Hou, J.J. Ge, J. Zeng, Q. Li, D.H. Reneker, A. Greiner, S.Z.D. Cheng, Chem. Mater. 17 (2005) 967–973.
[14] C. Kim, K.S. Yang, Appl. Phys. Lett. 83 (2003) 1216–1218.
[15] D. Li, Y.N. Xia, Adv. Mater. 16 (2004) 1151–1170.
[16] X.F. Lu, Y.Y. Zhao, C. Wang, Adv. Mater. 17 (2005) 2485–2488.
[17] P. Poizot, S. Laruelle, S. Grugeon, L. Dupont, J.M. Tarascon, Nature 407 (2000) 496–499.
[18] W.Y. Li, L.N. Xu, J. Chen, Adv. Funct. Mater. 15 (2005) 851–857.
[19] J. Chen, L.N. Xu, W.Y. Li, X.L. Gou, Adv. Mater. 17 (2005) 582–586.
[20] J. Hu, H. Li, X. Huang, Electrochem. Solid-State Lett. 8 (2005) A66–A69.
[21] J. Fan, T. Wang, C. Yu, B. Tu, Z. Jiang, D. Zhao, Adv. Mater. 16 (2004) 1432–1436.
[22] Y. Wang, J.Y. Lee, H.C. Zeng, Chem. Mater. 17 (2005) 3899–3903.
[23] L. Wang, Y. Yu, P.C. Chen, C.H. Chen, Scripta Mater. 58 (2007) 405–408.
[24] A.T. Serkov, Fibre Chem. 39 (2007) 60–63.
[25] R.Y. Hong, T.T. Pan, Y.P. Han, H.Z. Li, J. Ding, Sijin, J. Han, Magn. Magn. Mater. 310 (2007) 37–47.
[26] G. Sandi, R.E. Winans, K.A. Carrado, J. Electrochem. Soc. 143 (1996) L95–L98.
[27] N. Takami, A. Satoh, T. Ohsaki, M. Kanda, J. Electrochem. Soc. 145 (1998) 478–482.
[28] P. Poizot, S. Laruelle, S. Grugeon, J.M. Tarascon, J. Electrochem. Soc. 149 (2002) A1212–A1217.
[29] I.A. Courtney, J.R. Dahn, J. Electrochem. Soc. 144 (1997) 2045–2052.
[30] J.S. Xue, J.R. Dahn, J. Electrochem. Soc. 142 (1995) 3668–3677.
[31] C. Kim, K.S. Yang, J.Y. Kim, M. Endo, J. Mater. Sci. 38 (2003) 2987–2991.
[32] C. Kim, K.S. Yang, M. Kojima, K. Yoshida, Y.J. Kim, Y.A. Kim, M. Endo, Adv. Funct. Mater. 16 (2006) 2393–2397.
[33] J.S. Gnanaraj, M.D. Levi, E. Levi, G. Salitra, D. Aurbach, J.E. Fischer, A. Claye, J. Electrochem. Soc. 148 (2001) A525–A536.
[34] Y. Yu, Y. Shi, C.H. Chen, Nanotechnology 18 (2007), Art. No. 055706.
[35] Y. Yu, Y. Shi, C.H. Chen, C.L. Wang, J. Phys. Chem. C (2008), ASAP Article. doi:10.1021/jp800071h.
[36] M.S.A. Rahaman, A.F. Ismil, A. Mustafa, Polym. Degrad. Stabil. 92 (2007) 1421–1432.